

# Upper-Limb Powered Exoskeleton Design

Joel C. Perry, Jacob Rosen, *Member, IEEE*, and Stephen Burns

**Abstract**—An exoskeleton is an external structural mechanism with joints and links corresponding to those of the human body. With applications in rehabilitation medicine and virtual reality simulation, exoskeletons offer benefits for both disabled and healthy populations. A pilot database defining the kinematics and dynamics of the upper limb during daily living activities was one among several factors guiding the development of an anthropomorphic, 7-DOF, powered arm exoskeleton. Additional design inputs include anatomical and physiological considerations, workspace analyses, and upper limb joint ranges of motion. The database was compiled from 19 arm activities of daily living. The cable-actuated dexterous exoskeleton for neurorehabilitation (CADEN)-7 offers remarkable opportunities as a versatile human-machine interface and as a new generation of assistive technology. Proximal placement of motors and distal placement of cable-pulley reductions were incorporated into the design, leading to low inertia, high-stiffness links, and backdrivable transmissions with zero backlash. The design enables full glenohumeral, elbow, and wrist joint functionality. Potential applications of the exoskeleton as a wearable robot include: 1) a therapeutic and diagnostics device for physiotherapy, 2) an assistive (orthotic) device for human power amplifications, 3) a haptic device in virtual reality simulation, and 4) a master device for teleoperation.

**Index Terms**—Activities of daily living (ADLs), cable-actuated dexterous exoskeleton for neurorehabilitation (CADEN)-7, exoskeleton design, human arm, wearable robotics.

## I. INTRODUCTION

**T**HE EXOSKELETON is an external structural mechanism with joints and links corresponding to those of the human body. Worn by the human, the exoskeleton transmits torques from proximally located actuators through rigid exoskeletal links to the human joints. The same device with different control algorithms may be used in four fundamental modes of operation.

- 1) *Physiotherapy*: The patient wearing an exoskeleton performs task-based occupational or physical therapy in an active or passive mode [1]–[5].
- 2) *Assistive device (human amplifier)*: The operator feels scaled-down loads while interacting with objects in the environment, most of the load being carried by the exoskeleton [6], [7].
- 3) *Haptic device*: The subject physically interacts with virtual objects while the forces generated through the interactions

are fed back to the user through the exoskeleton conveying shape, stiffness, texture, or other characteristics of the virtual objects [8], [9].

- 4) *Master device*: Replacing the virtual environment with a real robot, the operator uses the exoskeleton to control a robotic system in a teleoperation (master/slave) mode, where the exoskeleton reflects back to the user the forces generated as the slave robot interacts with the environment [10], [11].

The previous two generations of this research effort consisted of 1-DOF and 3-DOF proof-of-concept prototypes. Although much less complex from both mechanical and control standpoints, they convincingly demonstrated that a novel method of higher level control using surface electromyographic (sEMG) signals as the primary command signal was viable [12], [13].

The objective of the current study was to design an anthropometric 7-DOF powered exoskeleton system, termed cable-actuated dextrous exoskeleton for neurorehabilitation (CADEN)-7. The anthropomorphic nature of the joints combined with negligible backlash in seven force-reflecting articulations sets the CADEN-7 apart from other arms in the field. The nearest design, the 7-DOF version of the PERCRO arm [8], utilizes two nonanthropomorphic joints to represent motion of the wrist and fingertips, and uses a closed mechanical human-machine interface (mHMI) around the forearm. It also appears to lack physiological motion in shoulder extension, although actual achievable ranges of motion (ROMs) are not reported. Other state-of-the-art arms lack one or more of the following: low-backlash gearing [10], [11], backdrivable transmissions [7], [10], low-inertia links [7], [9], [10], high-stiffness transmissions [11], open mHMIs [8], [9], or physiological ROMs [3], [4], [6]–[11].

The human-machine interface (HMI) of the operator/exoskeleton is designed to generate natural operation of the device. Given the exoskeleton mechanism and the selected application, various control algorithms were proposed (position, force-impedance). To trigger motion in the exoskeleton, these control strategies require the operator to either move part of his/her upper limb, or apply a force on the exoskeleton system. Under a neural control implementation, the neural HMI (nHMI) is set at the neuromuscular level of the human physiological hierarchy, using processed sEMG signals as one of the primary command signals to the system. Incorporating muscle models (myoprocessor) and taking advantage of the inherent electromechanical time delay in human neuromusculoskeletal physiology, the system can predict the operator's intention prior to the onset of movement, and thereby seamlessly integrate the operator and exoskeleton [14], [15].

The design and development of a high-performance robotic device is a process with numerous competing factors. Mechanism weight and stiffness exist at opposite ends of the spectrum.

Manuscript received November 28, 2006; revised April 6, 2007. Recommended by Guest Editors P. Dario and A. Menciassi. This work was supported in part by the National Science Foundation under Grant 0208468 entitled "Neural Control of an Upper Limb Exoskeleton System" to J. Rosen (PI).

J. C. Perry was with the Department of Mechanical Engineering, University of Washington, Seattle, WA 98195 USA. He is now with the Department of Electrical Engineering, University of Washington, Seattle, WA 98195 USA (e-mail: jcperry@u.washington.edu).

J. Rosen is with the Department of Electrical Engineering, University of Washington, Seattle, WA 98195 USA (e-mail: rosen@u.washington.edu).

S. Burns is with the Department of Rehabilitation Medicine, University of Washington, Seattle, WA 98195 USA (e-mail: spburns@u.washington.edu).

Digital Object Identifier 10.1109/TMECH.2007.901934

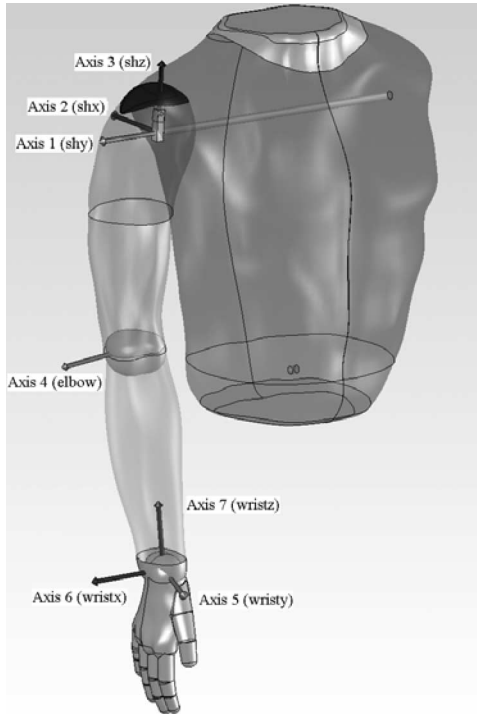


Fig. 1. Assignment of Euler  $Y-X-Z$  axes for the Vicon system. Human model from BodyWorks (Zetec Limited, New Zealand).

Contributing to these underlying requirements are factors such as the operational workspace, desired joint torques, motor placement, link design, and cable selection.

The design of the system was guided by experimental results of a research study on the kinematics and dynamics of the human arm in daily living activities. Details of the pilot study are explained in Section II, followed by a description of the resulting design requirements and additional system requirements in Section III. A detailed discussion of exoskeleton design considerations can be found in Section IV.

## II. PRELIMINARY INVESTIGATION—ADL PILOT STUDY

To better understand kinematic and dynamic requirements of an exoskeleton arm for functional use, a pilot study was first performed.

### A. ADL Materials and Methods

Motions of the human arm were recorded during 19 activities of daily living (ADLs) using a motion capture system (Vicon, 10 cameras). Captured activities were selected from the following task categories: general reaching tasks, functional tasks, eating and drinking, and hygiene-related tasks. Additional details of the study can be found in [15]. Frame assignments for the data collection are illustrated in Fig. 1.

Torques were calculated using two methods: a modeling simulation package (Cosmos/Motion, Solidworks) and an analytical approach (Autolev, Online Dynamics). In both cases, a 7-DOF model of the arm was used corresponding to the frame assignments of Fig. 1.

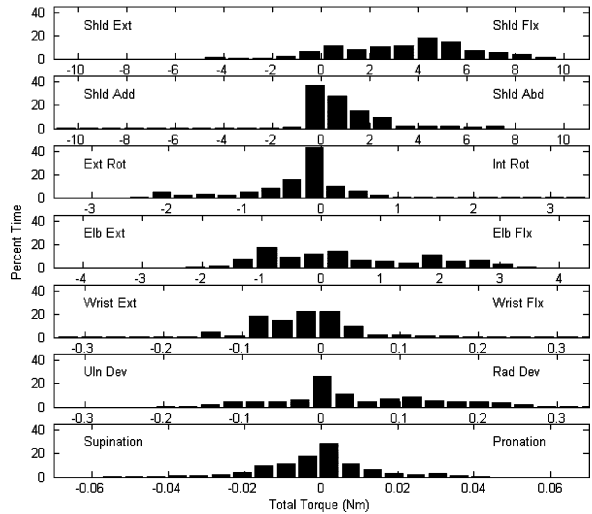
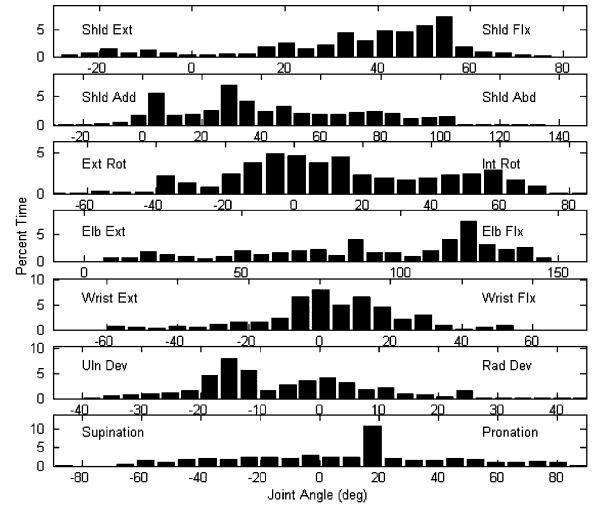


Fig. 2. Statistical distribution of human arm joint angles (top) and joint torques (bottom) during 19 ADLs [15]. Histograms are plotted sequentially from the top: Vicon axes 1 through 7—see Fig. 1. Zero position of the arm shown in Fig. 1.

### B. ADL Results

Results of joint position and joint torque distribution of the entire database about each axis are plotted in Fig. 2. While some distributions appear normal in shape, others possess bimodal or even trimodal forms where modal centers correspond to key anthropomorphic configurations. These configurations are positions of the arm that occur commonly throughout daily activities, often where joint velocities are low at the initial or final periods of motion trajectories.

## III. SYSTEM REQUIREMENTS

### A. Kinematic and Dynamic Requirements

Based on the results of the ADL pilot study, a table expressing the workspace and torque requirements of an assistive robot was generated (Table I). It is worthy to note that the largest required ROMs are found in elbow flexion–extension and forearm

TABLE I  
KINEMATIC AND DYNAMIC JOINT DESIGN REQUIREMENTS

MEASURE	VICON AXIS						
	1	2	3	4	5	6	7
Angle (deg)							
ROM	110	100	135	150	115	70	150
Mean	42.0	35.4	13.1	92.1	3.1	-4.8	11.7
Median	35.1	41.4	9.1	98.6	3	-9.3	15.9
Torque (Nm)							
Mean	3.5	1.0	-0.3	0.45	-0.02	0.04	0.00
Median	3.9	0.4	-0.1	0.18	-0.02	0.02	0.00
RMS	4.4	1.6	0.7	1.4	0.07	0.11	0.01

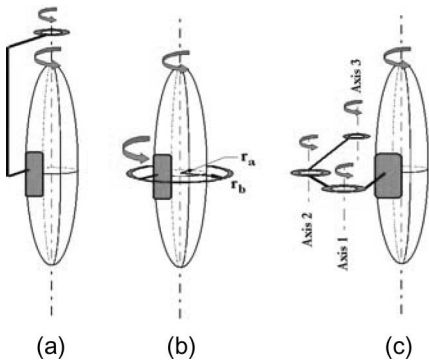


Fig. 3. Three exoskeleton configurations that achieve rotation about the long axis of a limb segment. (a) Proximally placed single DOF. (b) Circumferentially placed single DOF. (c) Three parallel, noncollinear DOFs.

pronosupination, each at  $150^\circ$ , while the requirement from shoulder flexion–extension, the joint having the largest physiological ROM, remains less at  $110^\circ$ . Average joint torques seen in the elbow and wrist are approximately one-tenth and one-hundredth, respectively, of those experienced at the shoulder, with median torques at the shoulder ranging from 0.4 to  $4 \text{ N} \cdot \text{m}$ .

### B. Mechanical Human–Machine Interfaces

The mHMIs are the physical components that mechanically couple the human arm and the exoskeleton structure, and enable force transmission between them. With awareness that one intended population of users will possess varying levels of muscular and functional impairment, an emphasis was placed on designing an interface that can easily be attached to the user. For patients of stroke and cervical spine injury, unassisted elevation of the arm is difficult, if not impossible.

To achieve axial rotation of exoskeleton limbs, three primary exoskeletal configurations are conceivable, illustrated in Fig. 3. The first two configurations involve a single-DOF bearing with its axis of rotation aligned collinearly with the approximate anatomical axis of rotation of the segment, while the third configuration involves a first axis that is displaced from the anatomical axis and a minimum of two additional noncollinear axes. In the first two configurations, the exoskeleton joint can be placed at either end of the long axis of the segment [Fig. 3(a)] or axially between the ends of the segment [Fig. 3(b)], using a bearing of minimum radius  $r_b$  greater than the maximum anthropometrical radius  $r_a$  about the corresponding segment axis. The additional

axes of the third configuration are required to correct for non-collinearity of the first axis with respect to the rotating segment.

The configuration shown in Fig. 3(a) offers a simple solution that allows for proximal placement of heavy components such as bearings and actuators, reducing inertial effects on power consumption; however, the placement is undesirable due to human–machine interferences during shoulder abduction. Configuration in Fig. 3(c) can avoid the interferences by displacing the joint axis laterally from the segment axis of rotation. However, the two additional joints, adding undesired weight and complexity to the design, are necessary to maintain proper rotation as was achieved in previous configurations through the use of a single joint. The second configuration [Fig. 3(b)] offers an alternative single-DOF solution where the human–machine interferences associated with the configuration shown in Fig. 3(a) can be removed. Full  $360^\circ$  bearings in this arrangement interfere with the torso when the arm is at rest or during motions that place distal arm joints near the body. Alternatively, these interferences can be removed through substitution of the full bearing with a partial bearing where the bearing track is affixed to the proximal exoskeleton link.

Current strength-to-weight limitations of available hardware necessitate immobile platforms for immediate upper limb exoskeleton technologies, and consequently, more user-friendly mHMIs. Strength-to-weight ratios of existing materials and electric motors, as well as energy-to-weight ratios of power supplies are not yet at the level necessary to support the development of mobile platforms for partial-body upper limb exoskeletons. As a result, a full-body exoskeleton is required to support the existing weight of state-of-the-art power supplies, onboard controllers, and other upper-limb hardware.

In the use of immobile platforms for therapy applications, positioning the device relative to an immobile arm to facilitate sleeve-like donning through closed ( $360^\circ$ ) bearings is less desirable, and joint configurations should be carefully selected and designed to minimize strain or discomfort to the user. Optimal designs for functionally impaired users enable the attachment of the arm and device with minimal movement of the impaired limb. Given a configuration that meets this criteria, additional codependent considerations such as link excursion, energy consumption, and collision avoidance with the body should be taken into account.

### C. Safety Requirements

Paramount to HMIs is the guarantee of safe operation. Safety precautions have been implemented on three levels, built into the mechanical, electrical, and software designs. In the mechanical design, physical stops prevent segments from excessive excursions that could hyperextend or hyperflex individual joints. The electrical system is equipped with three emergency shutoff switches: an enable button that terminates the motor command signal upon release, a large e-stop button for complete power shutoff by the observer, and a similar e-stop foot switch for the user.

Ideally, the aforementioned safety measures would go unused as a result of adequate safeguards at the software level.

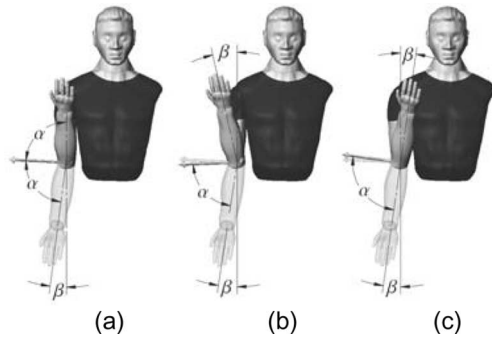


Fig. 4. Angular variations between elbow flexion–extension and pronosupination axes  $\alpha$  result in different elbow flexion kinematics. Type I individuals (a) are most common in which the elbow axis is symmetric with respect to both upper and lower arm segments. Types II (b) and III (c) are less common. Figure and types I–III designations adapted from [18].

Redundant position sensors (potentiometer, Midori, Fullerton; shaft encoder, HP), one at either end of the power train, monitor both joint motion and motor position. Redundancy of position sensing enables software to monitor power transmission integrity. A transmission slip, occurring between the motors and end effector, will result in a position discrepancy, and lead to immediate system shutdown. A shutdown request from any safety subsystem will engage brakes on motion of the shoulder and elbow. Software limits will also be implemented on commanded motor currents, i.e., motor torques.

#### D. Modeling the Human Arm

Anthropomorphic joint approximations can be modeled at varying degrees of accuracy and complexity [16]–[18]. The level of complexity needed for a suitable representation depends highly on the desired tasks to be performed and replicated using the model. Shoulder motion, for example, composed of glenohumeral (G-H), acromioclavicular, and sternoclavicular articulations, can be represented largely by the G-H joint for a variety of arm activities involving up to  $90^\circ$  of arm elevation. With minimal activity exceeding this range, a simplified model of the shoulder was deemed appropriate for the study. The G-H movement can further be simplified to a ball and socket joint composed of three orthogonal axes intersecting at the center of the humeral head, although the true center of rotation is known to vary with arm orientation [17], [18]. Rotations about these orthogonal axes may be treated as Euler rotation. The order of flexion–extension and abduction–adduction about the first two axes is arbitrary but should be noted, while the third rotation corresponds to internal–external rotation.

The elbow can be represented as a single-axis hinge joint where the hinge rests at an oblique angle with respect to both upper and lower arm segments under full-arm extension, as shown in Fig. 4. Of the three elbow types identified in [18], type I [Fig. 4(a)] is the most common, and was assumed in this analysis to represent the population. The hinge offset accounts for lateral deviation of the forearm during supinated activities. Under full-elbow extension and forearm supination, angular differences  $\beta$  of up to  $10^\circ$  exist between the midlines of the upper and

TABLE II  
TARGET VALUES FOR DESIGN PERFORMANCE

Property	Target Value
Weight (moving links)	6.8 kg (15 lbs)
Static Payload (max)	2.5 kg (in hand)
Angular Deflection (max)	2 degrees per joint
Bandwidth	0-10Hz

lower arm segments, and decrease with pronation. In the present study, an assumed offset of  $0^\circ$  has achieved sufficient results, and significantly reduced complexity of the resulting dynamic equations of motion.

Pronosupination of the forearm has been treated interchangeably in literature as a freedom of the elbow and as a freedom of the wrist. In either case, it should be considered directly adjacent to the forearm, occurring after elbow flexion and before either wrist flexion or deviation, with the axis of rotation running approximately through the fifth metacarpal–phalangeal joint [18].

The wrist can be modeled as two orthogonal axes with a fixed offset between them [18]. The proximal and distal axes of the wrist correspond to wrist flexion–extension and wrist radial–ulnar deviation, respectively.

#### E. Performance

A widely used quantitative measure to evaluate system performance is bandwidth. Systems having a higher bandwidth are controllable under higher frequency command signals. Limited by the system’s lowest natural frequency, the bandwidth is a measure of how successfully tradeoffs between weight and stiffness are made. A target bandwidth of 10 Hz was selected based on the achievable frequency range of the human arm, which resides between 2 and 5 Hz [19], [20]. Additional target values for the design are outlined in Table II. The actual weight was 3.5 and 6.3 kg for link 1 and links 2–7, respectively. Some preliminary experimental results of the exoskeleton are presented in Section IV-F.

## IV. EXOSKELETAL JOINT DESIGN

Articulation of the exoskeleton is achieved about seven single-axis revolute joints: one for each shoulder abduction–adduction (abd-add), shoulder flexion–extension (flx-ext), shoulder internal–external (int-ext) rotation, elbow flx-ext, forearm pronation–supination (pron-sup), wrist flx-ext, and wrist radial–ulnar (rad-uln) deviation. The exoskeletal joints are labeled 1 through 7 from proximal to distal in the order shown in Fig. 5. Note that the order and orientation of some joints are different from the axes presented in Fig. 1. Joint orientations are further addressed in Section III-D.

#### A. Anthropomorphic Joints

In the design of the current exoskeleton, three joint configurations emerged. The configurations can be classified as one of the following: 1)  $90^\circ$ ; 2)  $180^\circ$ ; or 3) axial.

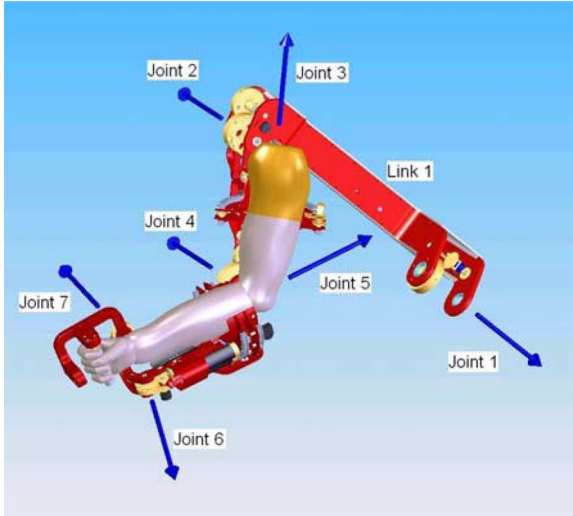


Fig. 5. CAD model (Solidworks, Concord) of exoskeletal axes assignment in relation to the human arm. Positive rotations about each joint produce the following motions: 1) combined flx/abd; 2) combined flx/add; 3) int rotation; 4) elbow flx; 5) forearm pron; 6) wrist ext; and 7) wrist radial deviation.

The distinction pertains to the relative alignment of adjoining links when the joint is approximately centered within its ROM. While some joints of the body articulate about their mid-ROM when adjoining links are near orthogonal [Fig. 6(a)], others do so when the links are near parallel [Fig. 6(b)]. A third configuration emerges in axial rotation of both the upper and lower arm segments [Fig. 6(c)]. As illustrated in Fig. 6(d), exoskeleton joints 1 and 7 are modeled as  $180^\circ$  joints, joints 2, 4, and 6 are  $90^\circ$  joints, and joints 3 and 5 are axial joints. Joint ROM in configurations 1) and 2) can be increased either by increasing the central radius  $r$  or decreasing the link width  $w$  [Fig. 6(a)]. Adjusting the link offset distance  $d$  shifts the joint limits, indicated in Fig. 6(a) and (b) by semitransparent circular markers, and effectively “tunes” the joint’s mid-ROM.

Consistent with other work, the G-H joint is modeled as a spherical joint composed of three intersecting axes [16]. The elbow is modeled by a single axis orthogonal to the third shoulder axis. Exoskeletal pronosupination takes place between the elbow and wrist joints as it does in the physiological mechanism. And finally, two intersecting orthogonal axes represent the wrist.

### B. Human–Machine Interfaces

The joint configuration shown in Fig. 6(c) presents special challenges in design as a result of the human arm occupying the joint axis of rotation, represented by the elliptical shape in Fig. 6(c) (top). Occurring in axial rotations of both the upper and lower arm, the exoskeleton mHMI uses a semicircular bearing design to allow users to don the device without strain or discomfort (Fig. 5). The semicircular guides are composed of three  $60^\circ$  curved rail bearing segments (THK, Tokyo, Japan).

### C. Joint Cable Routing

Achieving mechanical joint ROMs that match those of the human arm is a challenging task, especially in cable-driven devices where the cables must either be routed through or around

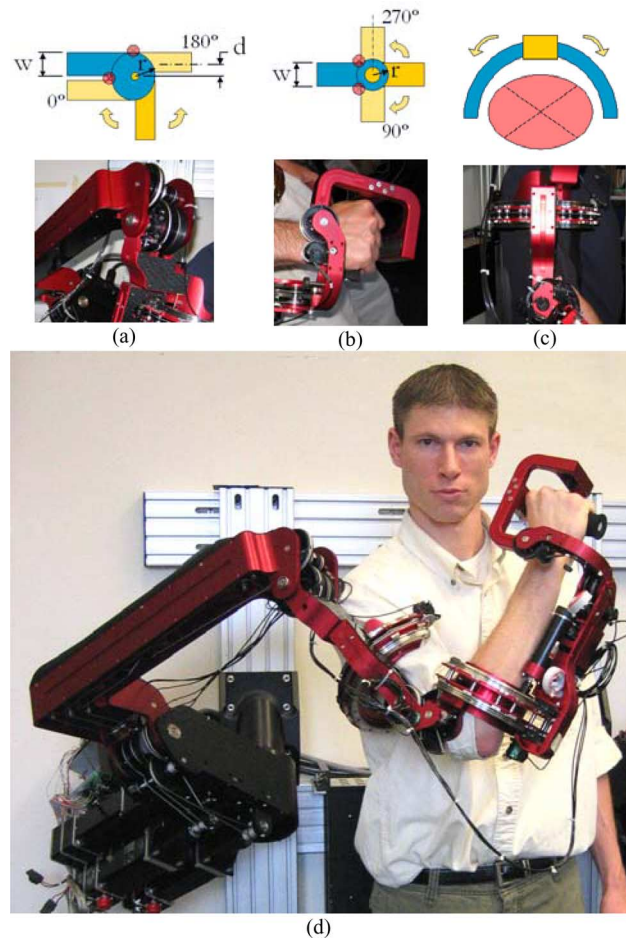


Fig. 6. Exoskeleton is composed of three joint configurations. (a)  $90^\circ$  joints. (b)  $180^\circ$  joints. (c) Axial joints. (d) Together the joints produce an exoskeleton structure that achieves full G-H, elbow, and wrist functionality.

TABLE III  
EXOSKELETON ACHIEVES 99% OF THE ROMS REQUIRED TO PERFORM DAILY ACTIVITIES

Joint	Motion	ADL ROM (deg)	EXO ROM (deg)
Shoulder	Flx-Ext	110	180
	Abd-Add	100	180
	Int-Ext Rot	135	166
Elbow	Flx-Ext	150	150
	Flx-Ext	115	120
Wrist	Rad-Uln Dev	70	60
	Pron-Sup	150	155

joint axes while maintaining constant cable length. The final cable routing arrangement enables ROMs that, in most cases, exceed ADL requirements (Table III).

The cable routing methods utilized are illustrated in Fig. 7. In  $90^\circ$  and  $180^\circ$  configurations, the cable is wrapped around a pulley, called the “joint idler pulley,” which is concentric with the axis of revolution [Fig. 7(a)]. Axial joints are represented by a series of nine idler pulleys each located at a constant radius

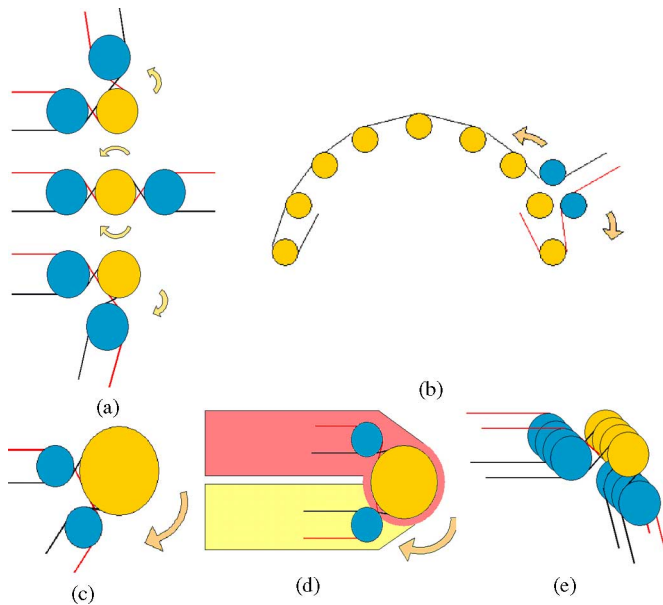


Fig. 7. Joint cable routing and the effects on ROM using (a) three equidiameter pulleys, (b) an enlarged joint pulley, or (c) an enlarged joint pulley and (d) link offset. Also, nine-pulley arrangement for axial joints (b) and cabling of stacked pulleys (e).

from the axis of revolution, together acting as a single larger diameter joint idler pulley [Fig. 7(b)].

To maintain constant cable length, the cable must remain in contact with the joint idler pulley at all times. The sequence shown in Fig. 7(a) shows the extent of joint motion using three equidiameter pulleys. At the extreme positions, the shorter length of cable is tangent with the joint idler pulley, and is therefore, defined as the joint limit. Fig. 7(c) illustrates the effect of increasing the joint idler pulley radius  $r$  on the amount of clockwise rotation before reaching the joint limit.

Fig. 7(d) depicts a  $90^\circ$  exoskeleton joint, and illustrates how an increased joint pulley radius  $r$  and offset  $d$  equal to  $r$  allow links to fold to an angle of  $0^\circ$ . Each pulley in the figure represents a stack of two pulleys per DOF passing through the joint. The 2-DOF case, for example, would require a stack of four pulleys [Fig. 7(e)], two pulleys representing the agonist muscle group and two pulleys representing the antagonist muscle group.

To enable bilateral routing of cables, as well as for lightweight strength, mechanical links were designed with high-stiffness I-beam cross sections. The I-beam channels were machined from aluminum stock, and custom pulleys were fastened directly to tapped holes in the beam for maximum transmission stiffness.

#### D. Singularity Placement

A singularity is a device configuration where a DOF is lost or compromised as a result of the alignment of two rotational axes. In the development of a 3-DOF spherical joint, the existence or nonexistence of singularities will depend entirely on the desired reachable workspace, where spherical workspaces equal to or larger than a hemisphere will always contain singular positions. The challenge is to place the singularity in an unreachable, or near-unreachable location, such as the edge of the workspace.

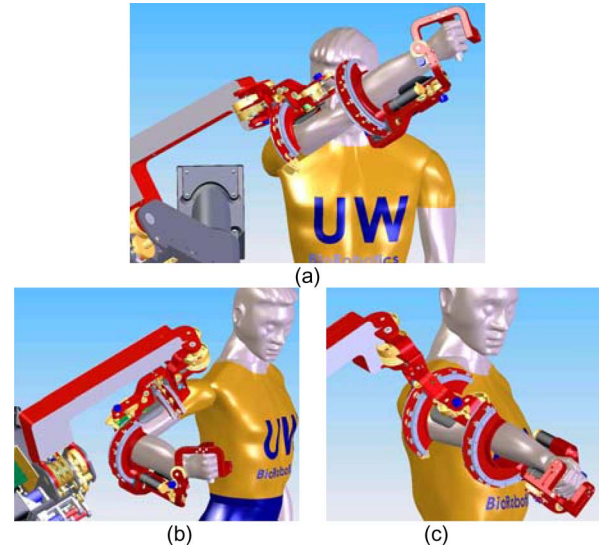


Fig. 8. Mechanical singularities between joints 1 and 3 occur around the shoulder int-ext rotation axis in configurations (a) and (b). A singularity between joints 3 and 5 also occurs in full elbow extension (c). Exoskeleton joints are labeled in Fig. 5.

For the exoskeleton arm, singularities occur when joints 1 and 3 or joints 3 and 5 align. To minimize the frequency of this occurrence, the axis of joint 1 was positioned such that singularities with joint 3 take place only at locations that are anthropometrically hard to reach. To allow some user-specific flexibility in the design, the singular position is movable in  $15^\circ$  increments. For the placement shown in Fig. 8, the singularity can be reached through simultaneous extension and abduction of the upper arm by  $47.5^\circ$  and  $53.6^\circ$ , respectively [Fig. 8(a)]. Similarly, the same singularity can be reached through flexion and adduction by  $132.5^\circ$  and  $53.6^\circ$ , respectively [Fig. 8(b)]. The singularity between joints 3 and 5 naturally occurs only in full elbow extension, i.e., on the edge of the forearm workspace [Fig. 8(c)]. With each of these singularity vectors at or near the edge of the human workspace, the middle and majority of the workspace is free of singularities.

Another aspect to consider when placing singularities is mechanical isotropy. For optimal ease of movement in any direction, singular axes should be placed orthogonal to directions where isotropy is of highest importance. For the singularity placement shown, isotropy will be maximized in  $42.5^\circ$  of shoulder flexion and  $26.4^\circ$  of shoulder abduction, values that lie in the median of the shoulder ROM as assessed from the ADL study.

#### E. Power Transmission

To date, the transmission of power from one location to another is achieved through a variety of means such as shafts, cables, fluid lines, and gear trains. Each method has specific applications where its characteristics are best suited. In the field of wearable robotics, weight is a critical factor that must be sacrificed frequently for the sake of strength or rigidity. However, the development of a rigid structure that lacks adequate

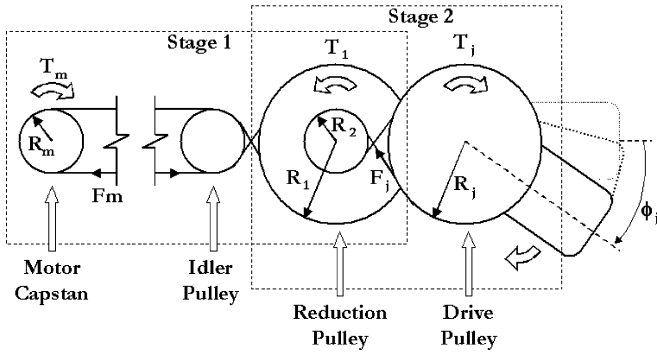


Fig. 9. Two-stage pulley reductions produce maximum transmission stiffness when length of high-tension stage 2 is minimized.

bandwidth is as ineffective a tool as one that is lightweight but lacks needed structural rigidity. To achieve both rigidity and bandwidth, critical decisions were made regarding transmission type and placement of actuators.

1) *Cable Drive Systems*: Cable drive systems have been in use on larger scale devices long before their introduction into the world of biorobotics and microsurgery. Their principal strength lies in their ability to transmit loads over long distances without the friction or backlash inherent to gears. The absence of backlash is achieved through the structural continuity of the cable, enabling a direct link between the driving shaft and the shaft or link being driven. For these reasons, a cable-driven design was selected. Biomimetically referred to as tendon drives, cable drives are common in robotic applications for their low backlash, and have been used by Salisbury *et al.* to achieve backdrivable speed reductions that increase the stiffness of the robotic structure [21]. This is discussed further in Section IV-E3.

2) *Selection and Placement of Actuators*: As the heaviest components in the design, placement of the motors was a crucial decision. Motors for joints 1–4 were mounted on the stationary base, achieving a 60% reduction in overall weight of the moving parts. The remaining three motors, whose torque requirements are substantially less, were positioned on the forearm. As each motor carries the weight and inertia of the more distally placed motors, the importance of high power-to-weight ratio increases from shoulder to wrist. Shoulder and elbow joints are each driven by a high torque, low power-to-weight motor (6.2 N·m, 2.2 N·m/kg), while wrist joints are driven by a lower torque, high power-to-weight motor (1.0 N·m, 4.2 N·m/kg). Motors are rare earth (RE), brushed motors (Maxon Motor, Switzerland).

3) *Two-Stage Pulley Reductions*: Pulley arrangements can be used to create speed reductions in cable transmissions. Neglecting frictional losses, power throughout the transmission remains constant while tradeoffs between torque and angular velocity can be made. At the motor, required torque is low while angular velocity is high, whereas at the joint, torque is high and angular velocity is low. Lower torque corresponds to lower cable tension in stage 1 (Fig. 9), resulting in less strain, and therefore, less stretch per unit length of cable. Minimizing the length of stage 2 and routing the cable in stage 1 through the majority of the robot maximizes the overall transmission

stiffness. Two-stage pulley reductions have been implemented in joints 1–4, whereas reductions at the wrist are composed of a single-stage pulley reduction following a single-stage planetary gear reduction. Total reductions for each joint are as follows: ~10:1 (joints 1–3), ~15:1 (joint 4), ~30:1 (joints 5–7).

4) *Cable Selection*: Steel cables, also referred to as wire rope, are available in a variety of strengths, constructions, and coatings. Although cable strength generally increases with diameter, the effective minimum bend radius is decreased. Cable compliance, cost, and construction stretch generally increases with strand count. A  $7 \times 19$  cable, composed of 133 individual strands, offers moderate strength and flexibility, and is recommended for use with pulleys as small as 25 times the cable diameter (SAVA Industries, Riverdale). Applications requiring high-strength cables and small-diameter pulleys, less than 1/25th the cable diameter, should utilize a higher count cable construction. The exoskeleton has been developed with both  $7 \times 19$  and  $7 \times 49$  cable constructions, where cable diameters were selected according to the following equations for cable stretch  $s$  and cable factor CF:

$$s = \left( \frac{0.0169F}{F_{BS}} + 0.0005 \right) L \quad (1)$$

$$CF = \frac{F}{D_c D_p} \quad (2)$$

where  $F$  is the cable tension,  $F_{BS}$  is the cable breaking strength,  $L$  is the cable length, and  $D_c$  and  $D_p$  refer to the outer and root diameters of the cable and pulley, respectively.

The cable tension  $F$  in (1) and (2) can be computed at the motor in stage 1,  $F_m$ , or at the joint in stage 2,  $F_j$ , based on the joint torque  $T_j$  using (3) and (4)

$$F_m = \frac{T_j}{N_2 R_1} \quad (3)$$

$$F_j = \frac{T_j}{R_j} \quad (4)$$

where  $N_2$  is the stage 2 pulley reduction,  $R_1$  is the radius of the larger diameter reduction pulley, and  $R_j$  is the radius of the drive pulley at the joint.

Optimal cable factors reported by SAVA for  $7 \times 19$  and  $7 \times 49$  cable constructions are less than 0.46 kg/mm<sup>2</sup> (650 lbs/in<sup>2</sup>) for nylon-coated cables, and decreases about a third using bare cable for a 2M cycle life. Note that CF is not a measure of tensile stress (pound-force per square inch) in the cable, but rather a measure of the accumulation of fatiguing stresses due to bending [see (2)].

#### F. Exoskeleton System Performance

It is known that system bandwidth is limited by a system's lowest natural frequency. To maintain performance, the lowest natural frequency of the exoskeleton should be above the highest frequency command signal generated by the human. As mentioned in Section III-E, achievable frequencies of the human arm range between 2 and 5 Hz [19], [20]. To measure resonant frequencies of the exoskeleton structure, an oscillating input with increasing frequency was given as a command to the system.

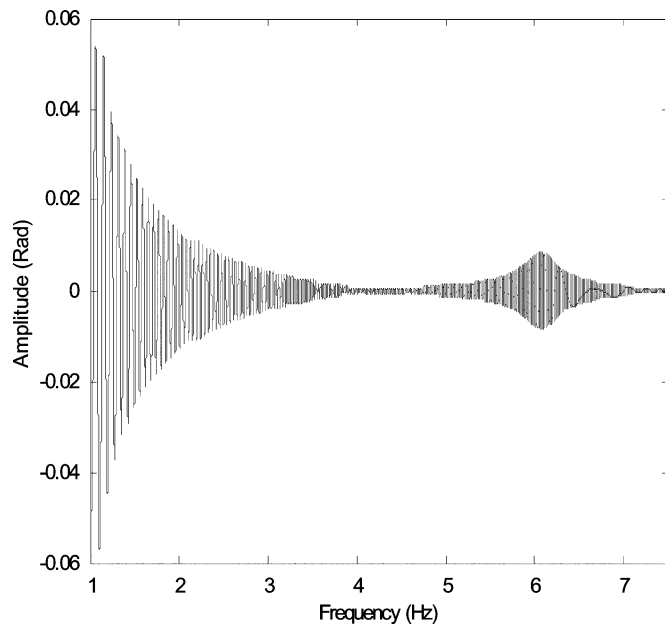


Fig. 10. Preliminary frequency response of exoskeleton joint 1 to a sinusoidal input wave varying in frequency from 1 to 8 Hz. Vertical axis shows the amplitude of the output (in radians).

The magnitude of the input was held constant, and the frequency increased at a rate of 0.1 Hz/s. Results indicate that the lowest resonant frequency occurs in the first shoulder joint (joint 1). Fig. 10 shows the first resonant mode of the exoskeleton at about 6 Hz.

Various preliminary control laws have been implemented on the exoskeleton. Fig. 11 shows joint responses to a step input using one such controller.

Recalling that measurement devices exist at both ends of the transmission (motor end: encoder, joint end: potentiometer), a mechanical input–output relationship for the exoskeleton can be seen in Fig. 11. Notice the close correlation during the initial response between encoder (dashed line) and potentiometer (dotted line) signals, particularly at the wrist, illustrating the high stiffness achieved by the transmission.

## V. DISCUSSION

From the study results presented in Section II, the largest ROM experience by a joint during the selected daily activities is  $150^\circ$ . Although some studies report joints to achieve ROMs exceeding  $180^\circ$ , most joints can only reach such excursions with contributions from neighboring joints. The G-H joint, for example, appears to provide over  $180^\circ$  of motion about all three axes; however, this is largely due to scapular motion. As a result, joints capable of providing  $180^\circ$  of motion, or less, in the configurations mentioned before are sufficient to develop an arm exoskeleton with full G-H, elbow, and wrist joint functionality.

It has been stated that to achieve proper correlation between Euler angle model representations and the actual biomechanics of the arm, forearm pronosupination should precede both wrist flexion and deviation axes. The reason for this is clear; however, this convention was not followed in the ADL pilot

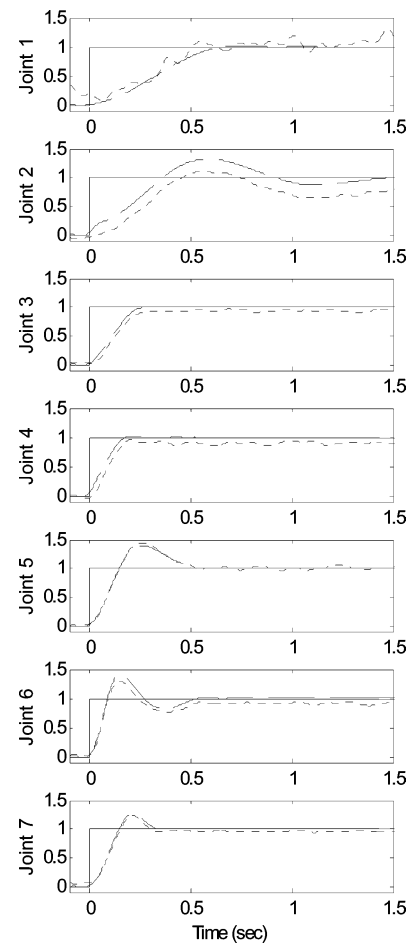


Fig. 11. System response—example response of individual exoskeleton joints to a step input. Traces are shown for the input step (solid), the output at the motor shaft (dashed), and the output at the joint (dotted). Note, the controller used here has not been optimized for system parameters.

study due to the existing convention of the modified plug-in-gait model that was used. As a result, the Vicon axes designated in Fig. 1 as 5, 6, and 7 cannot be directly compared to anatomical motions of wrist flexion, deviation, and rotation. They should instead be considered as a set, with axes 5 and 6 only corresponding to flexion–extension and radial–ulnar deviation when pronosupination is near zero, and axis 7 only corresponding to pronosupination when both wrist flexion and deviation are near zero. For purposes of the pilot study, this detail was deemed insignificant, since dynamic torques at the shoulder and elbow were the primary unknowns driving the motor requirements for joints 1–4, and ultimately the weight of the system.

Previous exoskeleton designs have primarily utilized internal–external rotation joints and pronosupination joints that fully enclose the arm, requiring the user to enter the exoskeleton from the device shoulder, and slide his/her arm axially down the length of the device through the closed circular bearings. This can be a difficult and even an uncomfortable task for users depending on the severity of impairment. In the current exoskeleton, the use of open mHMIs for both upper and lower arm segments eliminates this difficulty.

Due to the unique placement of the shoulder singularity, as described in Section IV-D, pure shoulder flexion is achieved through a combination of rotations about joints 1 and 2. Additionally, this unique placement moves the region of highest shoulder joint isotropy into the area of the workspace most often utilized during functional tasks. This further confirms that the singularity has been placed in an anthropometrically desirable location.

Cables throughout the design are terminated via multiple wraps around capstans of varying diameters. The movement of exoskeleton joints are achieved by wrapping of the cables at one end of the grooved capstans while simultaneously unwrapping at the other. This motion results in a lateral motion of the cables along the length of the capstans, accompanied by slight increases and decreases in cable length. Joint motions that cause significant changes in cable length will result in one of the two undesirable effects: either excessively high cable tension, reducing the life of the cables and bearings, or excessively low tension, potentially developing slack, transmission backlash, or even cable derailment. To prevent such occurrences, transjoint pulley arrangements are kept in contact with the joint pulley at all times, and lateral deviations of the cable at all cable termination sites were limited to  $2.5^\circ$ .

Although, anthropometrically, the wrist would be more accurately represented incorporating a slight offset between the flexion-extension and radial-ulnar deviation axes, this offset was neglected for simplicity. Unlike the neglected forearm offset  $\beta$ , which was unnoticeable to the user, the high sensitivity of the wrist joint to changes in position and torque make this human-machine discrepancy mildly noticeable. The wrist offset will be incorporated in future versions of the device.

As a final point of discussion regarding the 6-Hz mode of resonance, although this is below the target bandwidth proposed in Section III, the value remains sufficient for desired performance. It should be noted that the highest joint bandwidths in the human arm are found in distal limb joints, such as the wrist. Similarly, the same is true for the exoskeleton. Additionally, future work in controller optimization will produce significant decreases in both rise times and percent overshoot, as reported in Fig. 11.

## VI. CONCLUSION

In order to promote high performance while ensuring safe operation, the requirements for developing a 7-DOF exoskeleton must be realized and understood both from their technical as well as functional aspects. Additionally, the principles of physiological joints and cable-driven systems can assist in achieving a relatively lightweight, high-performance system. Proximal placement of motors, distal placement of pulley reductions, and open mHMIs are a few features that add to the performance and ease-of-use of the device. Additional characteristics include low inertias, high-stiffness links, and backdrivable transmissions without backlash. The design achieves full-workspace ROM, as defined by the ADL study.

Until higher power-to-weight ratio motors and structural materials are developed, the state-of-the-art in human strength wearable robotics will remain fixed either to immobile platforms

or to full-body support structures, such as powered wheelchairs or lower limb exoskeleton systems. Even within these technological constraints, however, upper limb exoskeletons have much to offer in regard to assistive and rehabilitative services, as well as in high-fidelity virtual simulations and advanced control applications.

## ACKNOWLEDGMENT

The authors wish to acknowledge L. M. Miller and T. M. Bardine-Fowler for their vital contributions to the work.

## REFERENCES

- [1] S. E. Fasoli, H. I. Krebs, J. Stein, W. R. Frontera, and N. Hogan, "Effects of robotic therapy on motor impairment and recovery in chronic stroke," *Arch. Phys. Med. Rehabil.*, vol. 84, pp. 477–482, 2003.
- [2] H. I. Krebs, B. T. Volpe, M. Ferraro, S. Fasoli, J. Palazzolo, B. Rohrer, L. Edelstein, and N. Hogan, "Robot-aided neuro-rehabilitation: From evidence-based to science-based rehabilitation," *Topics Stroke Rehabil.*, vol. 8, no. 4, pp. 54–68, 2002.
- [3] N. Hogan, H. I. Krebs, J. Charnnarong, P. Srikrishna, and A. Sharon, "MIT-MANUS: A workstation for manual therapy and training. I," in *Proc. IEEE Int. Workshop Robot Hum. Commun.*, Sep. 1992, pp. 161–165.
- [4] D. J. Reinkensmeyer, N. Hogan, H. I. Krebs, S. L. Lehman, and P. S. Lum, "Rehabilitators, robots, and guides: New tools for neurological rehabilitation," in *Biomechanics and Neural Control of Posture and Movement*, J. M. Winters and P. E. Crago, Eds. New York: Springer-Verlag, 2000, ch. 38.
- [5] R. Loureiro, F. Amirabdollahian, M. Topping, B. Driessen, and W. Harwin, "Upper limb robot mediated stroke therapy—GENTLE/s approach," *Special Issue Rehabil. Robot. J. Auton. Robots*, vol. 15, pp. 35–51, 2003.
- [6] D. W. Repperger, B. O. Hill, C. Hasser, M. Roark, and C. A. Phillips, "Human tracking studies involving an actively powered augmented exoskeleton," in *Proc. 15th Southern Biomed. Eng. Conf.*, 1996, pp. 28–31.
- [7] H. Kazerooni, "The human amplifier technology at the University of California, Berkeley," *Robot. Auton. Syst.*, vol. 19, pp. 179–187, 1996.
- [8] A. Frisoli, F. Rocchi, S. Marcheschi, A. Dettori, F. Salsedo, and M. Bergamasco, "A new force-feedback arm exoskeleton for haptic interaction in virtual environments," in *Proc. 1st Joint Eurohaptics Conf. Symp. Haptic Interfaces Virtual Environ. Teleoperator Syst.*, Mar. 2005, pp. 195–201.
- [9] M. Bergamasco, B. Allotta, L. Bosio, L. Bosio, L. Ferretti, G. Parrini, G. M. Prisco, F. Salsedo, and G. Sartini, "An arm exoskeleton system for teleoperation and virtual environments applications," in *Proc. IEEE Int. Conf. Robot. Autom.*, vol. 2, 1994, pp. 1449–1454.
- [10] B. M. Jau, "Anthropomorphic exoskeleton dual arm/hand telerobot controller," in *Proc. IEEE Int. Workshop Intell. Robots*, 1988, pp. 715–718.
- [11] D. G. Caldwell, O. Kocak, and U. Andersen, "Multi-armed dexterous manipulator operation using glove/exoskeleton control and sensory feedback," in *Proc. IEEE/RSJ Int. Conf. Intell. Robots Syst. 1995, Hum. Robot Interaction Cooperative Robots*, vol. 2, pp. 567–572.
- [12] J. Rosen, M. B. Fuchs, and M. Arcan, "Performances of hill-type and neural network muscle models—Toward a myosignal based exoskeleton," *Comput. Biomed. Res.*, vol. 32, no. 5, pp. 415–439, Oct. 1999.
- [13] J. Rosen, M. Brand, M. B. Fuchs, and M. Arcan, "A myosignal-based powered exoskeleton system," *IEEE Trans. Syst., Man, Cybern. A, Syst., Humans*, vol. 31, no. 3, pp. 210–222, May 2001.
- [14] E. Cavallaro, J. Rosen, J. C. Perry, S. Burns, and B. Hannaford, "Hill-based model as a myoprocessor for a neural controlled powered exoskeleton arm—Parameters optimization," in *Proc. IEEE Int. Conf. Robot. Autom. (ICRA 2005)*, Apr., pp. 4514–4519.
- [15] J. Rosen, J. C. Perry, N. Manning, S. Burns, and B. Hannaford, "The human arm kinematics and dynamics during daily activities—Toward a 7 DOF upper limb powered exoskeleton," in *Proc. 12th Int. Conf. Adv. Robot. (ICAR 2005)*, Jul., pp. 532–539.
- [16] B. A. Garner and M. G. Pandey, "A kinematic model of the upper limb based on the visible human project (VHP) image dataset," *Comput. Methods Biomech. Biomed. Eng.*, vol. 2, pp. 107–124, 1999.
- [17] B. F. Morrey and K. N. An, "Biomechanics of the shoulder," in *The Shoulder*, vol. 1, C. A. Rockwood and F. A. Matsen, Eds. Philadelphia, PA: Saunders, 1990, ch. 6.

- [18] I. A. Kapandji, *The Physiology of the Joints: Annotated Diagrams of the Mechanics of the Human Joints*, 5th revised ed. New York: Churchill Livingstone, 1982.
- [19] H. Kazerooni, "Human-robot interaction via the transfer of power and information signals," *IEEE Trans. Syst., Man, Cybern.*, vol. 20, no. 2, pp. 450–463, Mar./Apr. 1990.
- [20] T. L. Brooks, "Telerobotic response requirements," in *Proc. Int. Conf. Syst., Man, Cybern.*, Los Angeles, CA, Nov. 1990, pp. 113–120.
- [21] K. Salisbury, W. Townsend, B. Eberman, and D. DiPietro, "Preliminary design of a whole-arm manipulation system (WAMS)," in *Proc. IEEE Int. Conf. Robot. Autom.*, vol. 1, Apr. 1988, pp. 254–260.



**Joel C. Perry** was born in Bellingham, WA, in 1978. He received the B.Sc. degree from Gonzaga University, Spokane, WA, in 2000, and the M.Sc. and Ph.D. degrees from the University of Washington, Seattle, in 2002 and 2006, respectively, all in mechanical engineering.

From 2000 to 2002, he was a Research Assistant developing a powered prosthesis at the VA Hospital, Seattle. From 2002 to 2006, he was engaged in developing an anthropomorphic powered exoskeleton, and since 2006, has been developing medical robotics at

the Biorobotics Laboratory, Department of Electrical Engineering, University of Washington. His current research interests include medical device development, rehabilitation robotics, and assistive technologies for the disabled.



**Jacob Rosen** (M'01) received the B.Sc. degree in mechanical engineering and the M.Sc. and Ph.D. degrees in biomedical engineering from Tel-Aviv University, Tel-Aviv, Israel, in 1987, 1993, and 1997, respectively.

From 1993 to 1997, he was a Research Associate developing and studying the myosignal based powered exoskeleton at the Biomechanics Laboratory, Department of Biomedical Engineering, Tel-Aviv University. He was also a Biomechanical Engineer in a startup company where he was engaged

in developing innovative orthopedic spine/pelvis implants. Since 1997, he has been at the University of Washington, Seattle, where he is currently a Research Associate Professor of electrical engineering with adjunct positions in the Departments of Surgery and Mechanical Engineering. His current research interests include surgical robotics, wearable robotics (exoskeleton) biorobotics, biomechanics, and human-machine interface.



**Stephen Burns** received the B.Sc. degree in biology and the M.D. degree from Brown University, Providence, RI, in 1988 and 1992, respectively.

From 1992 through 1996, he completed residency training in physical medicine and rehabilitation, first at the University of Washington, Seattle, and later at Thomas Jefferson University, Philadelphia, PA. Since 1996, he has been a Staff Physician for the Spinal Cord Injury Center, VA Puget Sound Health Care System, Seattle. He is currently an Associate Professor in the Department of Rehabilitation Medicine,

University of Washington. His current research interests include respiratory complications associated with spinal cord injury, motor recovery following traumatic tetraplegia, and wearable robotics.

Prof. Burns serves on the Neurological Standards Committee of the American Spinal Injury Association, and is also a member of the American Paraplegia Society.